Analysis of Quantitative Prediction of Rib-Fractures using Finite Element Human Body Models during Side Impacts

Yasuki Motozawa, Masayoshi Okamoto, Fumie Mori

Abstract The objective of the present study was to examine the feasibility of probability-based methods in quantifying the risk of rib fractures using finite element (hereafter FE) human body models under various loading conditions during side impacts. A series of simulated side impact experiments were performed using fracture and non-fracture FE human body models placed in various seated positions. Simulations were performed in compliance with the IIHS SICE protocol. Five different seating positions were chosen for the simulations. The FE human body models used in the present study represent the anthropometry and material properties of 50th percentile American 75 year old males. The predicted risk of fractures in both models, i.e. simulated fractures in the fracture model and hotspots on the non-fracture model, were compared and analysed. The results indicated that the prediction of the first-phase fractures indicated good correlation for both models, whereas the non-fracture model did not represent the distribution of the second-phase fractures simulated by the fracture model.

Keywords FE human body model, post-fracture, probability, rib-fracture, side impact

I. INTRODUCTION

Due to recent changes in the population, age-related injuries have become an important issue. This can be explained by a decreased tolerance in the biological material of which human tissue consists. In particular, in comparison with other materials, the cortical bone shows a significant decrease in the value of maximum strain with age, and thus the elderly are more likely to suffer from bone fractures [1-2]. Among such fractures, rib fractures during vehicle impacts, which are frequently observed in elderly occupants, have become important issues because of the serious outcomes, despite the considerably low injury severity on the AIS scale [3]. Another noticeable physical change with age is that of skeletal geometry. The change of the curvature of the thoracic spine consequently yields a change in the angle of the costovertebral joints and in the geometry of the entire rib-cage. This observation suggests that the skeletal load-path and the distribution of strain may change with age; it possibly affects the distribution of fractures in the rib-cage. Analyses of thoracic injury mechanism in the elderly population or direct assessments of the risk of rib fractures have been difficult to perform using conventional Anthropomorphic Testing Devices (ATD) or generic human body finite element models (FE models), due to the limited bio-fidelity of the characteristics of the population.

In their previous studies, the authors established age-specific FE human body models, representing the anthropometry and material properties of 50th percentile American males aged 35 years old and 75 years old (YO), respectively, representing rib fractures by element elimination [4-8]. By using these models, the authors conducted a series of simulated pendulum impact tests on the thorax, consequently establishing a perspective of the distribution of regional thoracic stiffness in both populations [9]. Furthermore, they conducted a series of simulated side impact experiments and compared and analysed the whole body kinematics and predicted rib fractures in fracture and non-fracture FE human body models [10]. The results of their previous study indicated that the whole-body kinematics of the non-fracture models were almost identical to those of the fracture models. They also indicated that the distribution of hotspots (elements where strain reached a threshold i.e. predicted fractures) in the non-fracture model showed good correlation with those of simulated fractures in the

Y. Motozawa is Chief Engineer at Honda R&D Co., Ltd., Automobile R&D Center in Haga-gun, Tochigi, Japan (+81-80-9447-3816, yasuki_motozawa@n.t.rd.honda.co.jp). M. Okamoto is Assistant Chief Engineer at Honda R&D Co., Ltd. F. Mori is Engineer at Honda Techno Fort Co. Ltd. in Haga-gun, Tochigi, Japan.

fracture models. These results may support the appropriateness of the probability-based method for injury quantification using non-fracture models proposed by [11]. However, the simulated experiments in their previous study were conducted under very specific conditions; the loading condition on the thorax was limited in distributed loading mainly applied thorough thoracic side airbags. Owing to that, the authors were only able to examine the effect of the change of indirect loading, i.e. the influence of the primary fractures on the secondary fractures in one load-path (in a single rib), but could not examine conditions under which direct concentrated loading mainly contributed to fractures, or *chain-reactions*, i.e. successive fractures initiated by the primary fractures on other ribs.

The objective of the present study was to examine the feasibility of the probability-based methods to quantify the risk of rib fractures using FE human body models under various side-impact conditions. A series of simulated side impact experiments were performed using fracture and non-fracture FE human body models placed in various seated positions. The FE human body models used in the present study represent the anthropometry and material properties of 50th percentile American 75 YO males. The predicted risk of fractures on both models, i.e. simulated fractures in the fracture model and hotspots in the non-fracture model were compared and analysed.

II. METHODS

In the present study, the authors conducted performed side impact experiments using FE human body models placed in five different seated positions. The authors attempted to carry over the methodology of the previous study for direct comparison. Therefore, the FE human models, simulated test setup and test method other than seated positions are identical to the previous study [10]. However, the authors will describe the detailed methods for convenience.

Human Body Models

The FE human body models used in the present study represent the anthropometry and material properties of 50th percentile American 75 YO males (hereafter, FE elderly human body models). Table A I in the Appendix indicates the material material properties used in the FE elderly human body models. The models incorporated the lower limbs, lumbar spine and thorax models previously developed by [4-8]. In order to determine the geometry of the 75 YO rib-cage model, a specific CT image for the relevant age range that approximates American male 50th percentile was extracted from the medical database at the University of Michigan Program for Injury Research and Education (UMPIRE). Based on the image, an FE mesh of the 75 YO rib-cage model was created. In the model, the element size of the bones was between 2mm and 7mm. The model was compared to the statistical data from the previous study conducted by [12] and [13] and was found to indicate close match to the average geometry of the relevant age group. The remaining body regions, i.e. the head, neck and upper extremities, were supplemented by the H-Model^{TM}, which is a commercially available generic human body FE model consisting of 304,390 elements [14]. PAM-CRASH^{TM} (ESI Group, 100-102 Avenue de Suffren 75015 Paris, France) was used as the FEM solver. Figure 1 shows the FE elderly human body model. The responses of the thoracic component of both human FE models during pendulum impacts were validated against the results of published experiments performed by [15-16]. The responses during a table-top thoracic belt loading were also validated against the experiments performed by [17]. Previously, the authors simultaneously developed an FE human body model representing the anthropometry and material properties of 50th percentile American 35 YO males (hereafter, FE adult human body model) based on the identical CT image to the FE elderly human body models in the same manner. They compared the time histories of the displacement of the head, vertebral bodies and pelvis of the FE adult human body model to the averages of the sled experiments. They evaluated the bio-fidelity of the model using a ranking method proposed by [18]. Consequently, they successfully validated sufficient biofidelity of the model during frontal and side impacts. Table A II in the Appendix indicates the biofidelity scores of the FE adult human body model during side impacts.

Fig. 1. FE elderly human body model: skin is not displayed in the left side.

Test Set-up Models

The authors developed an FE model of the test set-up for a vehicle to moving deformable barrier (MDB) side-impact experiment. The model consists of a full-scale FE model of the vehicle body (vehicle model) and the MDB. The vehicle model represents a test set-up of a small sedan-type volume production vehicle (the Honda Civic), consisting of a whole-vehicle sheet-metal body structure (white-body), a frontal seat equipped with a thoracic side airbag, doors with plastic door trims and a set of seatbelts. However, the spool and the tension retractor of the seatbelt were omitted to obtain stable boundary conditions. Drive train components with an engine, the front and rear suspension systems with tyres, an engine hood, a trunk lid, glazing, bumper-face and interior trims other than door trims were omitted, but the respective masses of the omitted components were applied to the vehicle model so that the total mass and moment of inertia of the vehicle was maintained. The white-body structure, doors and door trims were modelled by shell elements. The seatbelts were modelled using bar and membrane elements in which the force-elongation properties of the actual material of the webbing used in the production vehicle were reflected. The padding of the front seat was modelled by solid elements and sculptured along the surface of the human FE models in the relevant seated position. The MDB model used in the present study was modeled to represent the MDB defined by the Side Impact Crashworthiness Evaluation Crash Test Protocol (SICE) determined by the Insurance Institute for Highway Safety (IIHS). The deformable structure (aluminum honeycomb) in the front end of the MDB was modelled as a solid element, but the other structure was modelled as a rigid body for simplification.

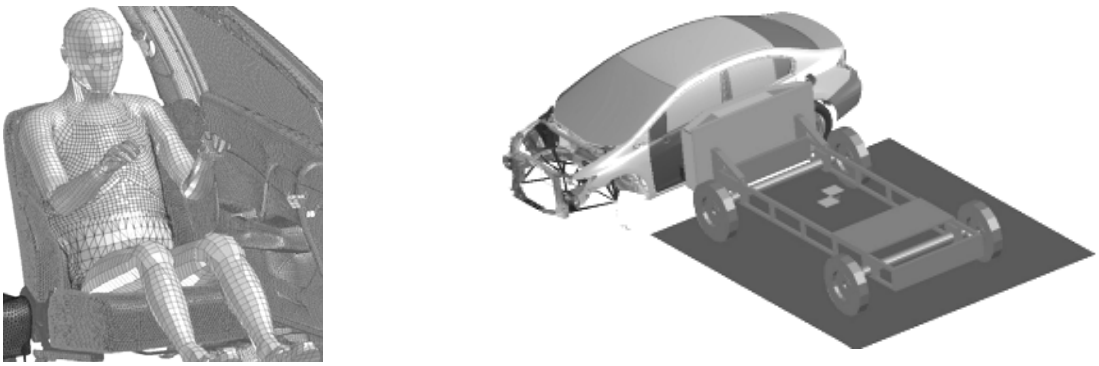

Fig. 2. FE Test set-up model accommodating the human FE model: The left figure indicates FE human body model placed in the vehicle model and the right image indicates the entire test set-up, consisting of the vehicle and MDB models based on the IIHS SICE protocol.

The authors conducted an FE simulation using the test set-up FE model accommodating a SID-IIs ATD FE model in the same manner as the SICE protocol, and the time histories of the local velocity of the vehicle model, and the velocity and the deflection of each rib of the SID-IIs ATD FE model during impact were calculated and compared to those of the experiment using an actual test set-up identical to the model. Figures A1 and A2 in the Appendix indicate the comparisons of the time histories of the local velocity of the vehicle. Since the results of the FE simulation showed a close match to the experimental results, the author deemed that the entire test set-up model was validated against the actual experiment.

Conditions of FE Simulation

Throughout the present study, PAM-CRASH^{TM} was used as the FEM solver as described above. The MDB model was collided with a stationary vehicle model holding the FE elderly human body model at an impact velocity of 50 km/h on the driver side at a 90-degree angle in the same manner as the SICE protocol. The respective FE elderly human body model was placed in the driver seat (left-side, i.e. near-side against the MDB). The human body model wore the seatbelts. The thoracic side airbag was activated at 7 ms from the initiation of the impact (hereafter, t=7 ms). The FE calculation was done up until t=80 ms. Five different seated positions were chosen for both fracture and non-fracture FE elderly human body models; 100 mm forward from neutral position, 45 mm forward from neutral position, neutral position i.e. baseline or identical to SICE protocol, 45 mm backward from neutral position and 100 mm backward from neutral position (hereafter, Cases 1, 2, 3, 4 and 5, respectively). Figure 3 shows the respective seated positions. At the seated position of Case 1, the upper torso of the human body model was in the closest position to the centre of the door where the deflection (intrusion) of the door inner panel was larger than other seated positions, whereas the upper torso of the human body model was in the closest position to the B pillar (centre pillar) of the vehicle model in Case 5. Figure 4 shows the status of the body structure, the door, the seat, the thoracic side airbag and the upper torso of the FE elderly human body model at t=30 ms in Case 3. The respective kinematics and the time histories of the strain on the ribs in both FE elderly human body models, hotspots in the non-fracture model, simulated fractures in the fracture model and the timing of the occurrence of simulated fractures, or hotspots were recorded. The authors defined primary fracture or hotspot as the simulated fracture or hotspot firstly observed in the respective ribs, and secondary fracture or hotspot in the same manner.

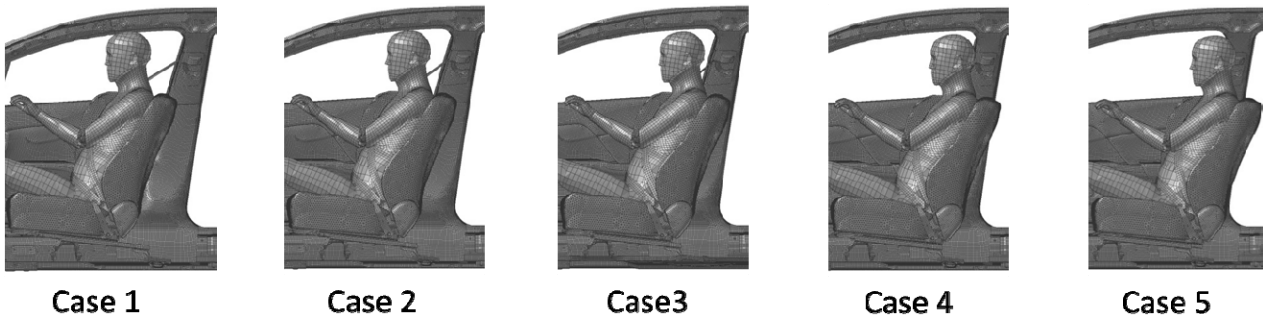

Fig. 3. Seated positions for respective impact conditions; 100 mm forward from neutral position, 45 mm forward from neutral position, neutral position (baseline), 45 mm backward from neutral position and 100 mm backward from neutral position (Cases 1, 2, 3, 4 and 5, respectively).

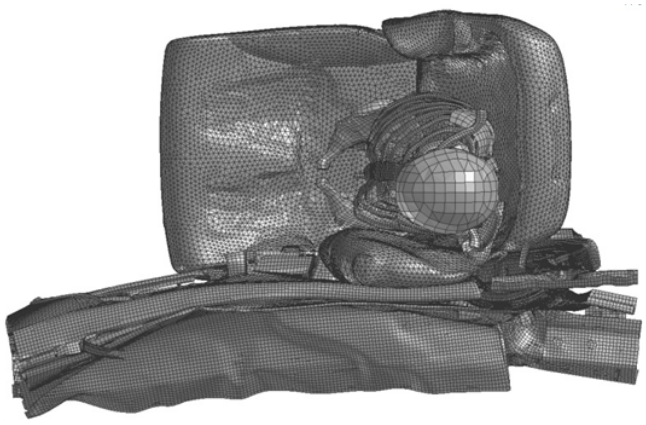

Fig. 4. Body structure, door, seat, thoracic side airbag and upper torso of FE elderly human body model at t=30 ms in Case 3; lower torso of the human body model is not displayed for convenience.

III. RESULTS

Figure 5 indicates distributions of the simulated fractures in the fracture model under each condition. Table I

shows the respective timing of the occurrence of the simulated fractures in the fracture model under each conditions. Figure 6 indicates hotspots in the non-fracture model in the same manner as Figure 5. Table II shows the respective timing of the occurrence of the hotspots in the non-fracture model in the same manner as in Table I. In Tables I and II, primary and secondary fractures and hotspots that occurred in a single rib were displayed. In these Tables, the authors defined *anterior* as the region within one third of the length of the respective ribs from the sternocostal joint, *posterior* as the region within one third of the rib length from the costovertebral joint and *side* as the remaining region. Figures 5 and 6 display the left side rib-cage; in the present study simulated fractures and hotspots were observed only in the left (impacted side). For convenience, body regions, internal organs, soft tissues and skins other than the thoracic skeleton are not displayed in These Figures.

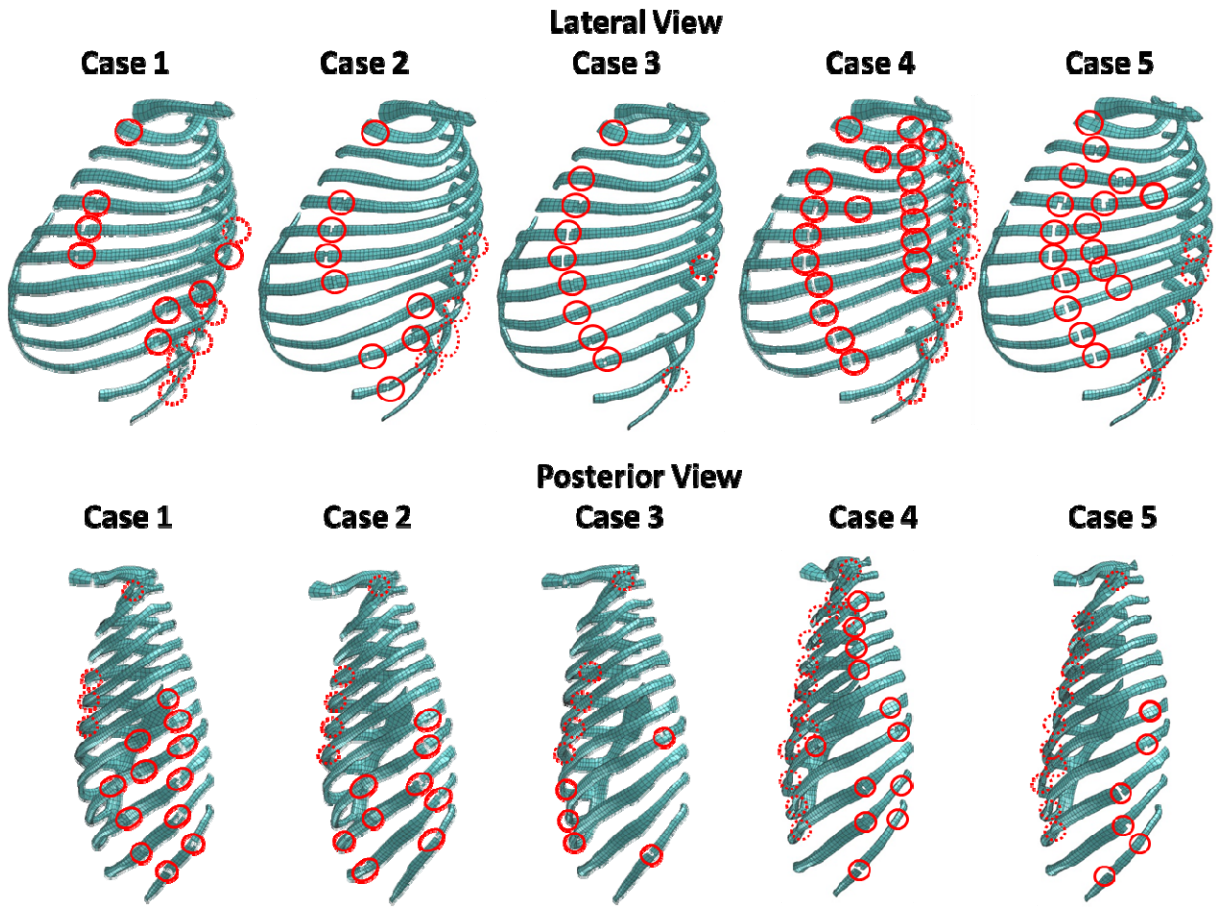

Fig. 5. Distributions of simulated fractures in fracture model: The circles in solid line indicate fractures and the circles in dotted line indicate fractures obscured by the ribs. Figure displays the left side rib-cage because simulated fractures were observed only in the left. Body regions, internal organs, soft tissues and skins other than the thoracic skeleton are not displayed.

TABLE I

TIMING OF OCCURRENCE OF SIMULATED FRACTURES IN FRACTURE MODEL (ms).

	Case 1				Case 2				Case 3				Case 4				Case 5			
Rib	**First**		**Second**		**First**		**Second**		**First**		**Second**		**First**		**Second**		**First**		**Second**	
R1	46.5	Anterior			49.0	Anterior			46.9	Anterior			23.5	Posterior	44.2	Posterior	21.9	Anterior		
R2													42.9	Side	42.9	Posterior	44.9	Anterior		
R3									43.8	Anterior			41.7	Anterior	42.7	Side	42.1	Anterior	42.7	Side
R4	28.7	Anterior			26.9	Anterior			26.4	Anterior			22.5	Side	24.1	Anterior	20.2	Anterior	22.7	Anterior
R5	26.4	Anterior			24.6	Anterior			24.0	Anterior			22.2	Anterior	43.9	Side	20.7	Anterior	48.6	Side
R6	26.9	Anterior			25.0	Anterior			23.8	Anterior			22.2	Anterior	44.1	Side	20.5	Anterior	46.5	Side
R7	34.9	Side			29.5	Anterior			27.0	Anterior			23.1	Side	44.5	Side	20.2	Anterior	20.9	Side
R8	27.7	Posterior	39.3	Posterior	29.1	Posterior							22.3	Side	38.9	Posterior	19.2	Anterior	19.4	Posterior
R9	25.3	Posterior	37.1	Side	25.5	Posterior	42.2	Posterior	32.3	Side	41.5	Posterior	21.1	Posterior	21.3	Posterior	18.7	Posterior	19.3	Side
R10	25.2	Posterior			26.4	Posterior	31.4	Side	30.0	Side			18.9	Side	24.0	Posterior	17.4	Posterior	17.6	Side
R11	25.9	Posterior	38.3	Side	24.9	Posterior	29.3	Side					25.5	Posterior	25.6	Posterior	18.4	Posterior		
R12	22.0	Side	28.6	Posterior	23.5	Posterior			18.0	Posterior			16.2	Posterior	27.3	Posterior	15.8	Posterior	26.9	Posterior

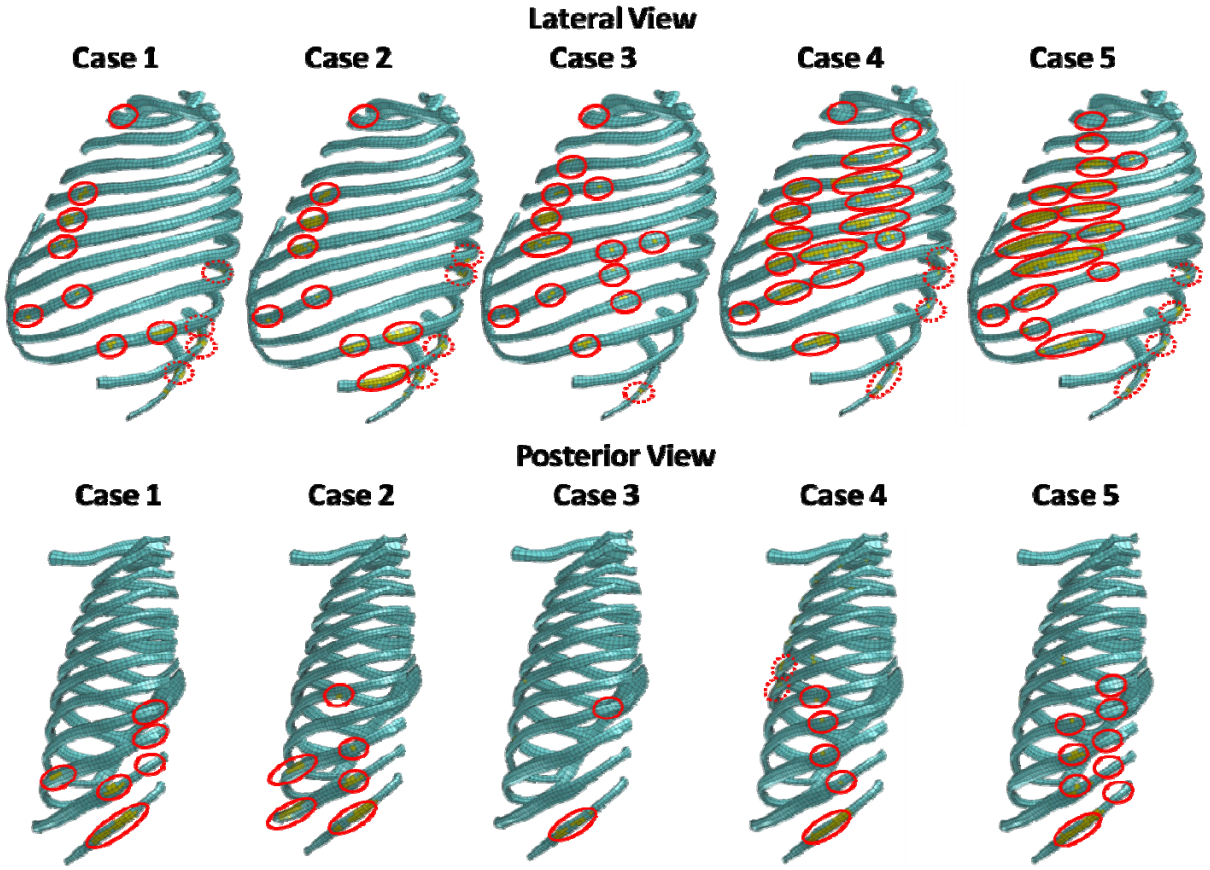

Fig. 6. Distributions of hotspots in non-fracture model: The circles in solid line indicate hotspots and the circles in dotted line indicate hotspots obscured by the ribs. Figure displays the left side rib-cage because hotspots were observed only in the left. Body regions, internal organs, soft tissues and skins other than the thoracic skeleton are not displayed.

TABLE II
TIMING OF OCCURRENCE OF HOTSPOTS IN NON-FRACTURE MODEL (ms).

	Case 1				Case 2				Case 3				Case 4				Case 5			
Rib	**First**		**Second**		**First**		**Second**		**First**		**Second**		**First**		**Second**		**First**		**Second**	
R1	51.9	Anterior			50.5	Anterior			51.1	Anterior			44.9	Anterior			45.5	Anterior		
R2													43.9	Posterior			43.5	Anterior		
R3									47.3	Anterior			43.9	Anterior	44.8	Side	43.1	Anterior	43.7	Side
R4	33.0	Anterior			30.2	Anterior			25.6	Side	29.4	Anterior	23.3	Side	27.0	Anterior	22.5	Side	46.3	Side
R5	29.6	Anterior			27.2	Anterior			27.3	Anterior			24.1	Anterior	43.8	Side	22.6	Anterior	47.0	Side
R6	31.1	Anterior			26.0	Anterior			25.3	Anterior			23.6	Anterior	43.6	Side	23.4	Anterior	46.2	Side
R7	34.9	Side							46.0	Posterior	49.0	Side	24.7	Side	29.0	Anterior	23.5	Anterior	24.0	Side
R8	30.9	Anterior			29.4	Anterior	31.6	Posterior	31.7	Anterior	49.9	Side	28.2	Anterior	44.0	Posterior	21.6	Posterior	25.6	Anterior
R9	34.0	Posterior			30.3	Posterior			42.0	Posterior	45.5	Side	24.7	Posterior			19.9	Anterior	21.5	Posterior
R10	29.1	Anterior	34.9	Posterior	29.9	Posterior	32.3	Side	30.2	Anterior			28.2	Anterior	29.4	Posterior	19.2	Posterior	19.5	Anterior
R11	32.6	Posterior	32.9	Posterior	29.3	Posterior	31.9	Posterior					25.8	Posterior			17.4	Posterior	25.3	Posterior
R12	24.5	Posterior	31.2	Posterior	27.0	Posterior	28.9	Posterior	27.2	Posterior	27.5	Posterior	18.3	Posterior			17.6	Posterior	26.0	Posterior

Table III indicates the number of fractured ribs and the total number of simulated fractures in the fracture model, as well as indicating the number of ribs with hotspots and the total number of hotspots in the non-fracture model for the five conditions used. In the non-fracture model, up to two hotspots, i.e. primary and secondary hotspots observed in a single rib, were recorded.

TABLE III
NUMBER OF FRACTURED RIBS AND TOTAL NUMBER OF SIMULATED FRACTURES OR HOTSPOTS

Condition	Case 1	Case 2	Case 3	Case 4	Case 5
Fractured Ribs in Fracture Model	10	10	10	12	12
Fractures in Fracture Model	16	13	11	23	23
Ribs with Hotspots in Non-fracture Model	9	9	10	12	12
Hotspots in Non-fracture Model	13	13	15	20	26

IV. DISCUSSION

First, the authors took a look at global trends in the distribution of simulated fractures in the fracture model. In the fracture model, simulated fractures occurred in the floating ribs (the 11th and 12th rib, hereafter, R11 and 12) very early on from the initiation of impact. Given the structure of the rib-cage, the fractures in the floating ribs would have contributed little to the fractures in the upper ribs (from R1 to 10). Therefore, hereafter the authors will focus on the upper ribs.

Next, the authors compared the distributions of the (simulated or predicted) fractures in both human models with the timing at which they occurred in Cases 1, 3 and 5. In Case 3, the observation of the simulated fracture in the fracture model at the time showed that primary fracture occurred on the anterior side of R6 at t=24 ms, followed by R5, 6, 7 and 8. In their previous study, the authors conducted simulated pendulum impact tests using the FE elderly human body model and established a map of the distribution of thoracic stiffness and hypothesized its mechanism [9]. Their findings showed that the load-transmission from the loaded ribs to the neighbouring ribs through the soft tissues is relatively small on the side thorax. Hence, the global stiffness (incline of force-deflection curve) of the rib-cage is smaller under concentrated loading on the side thorax than under distributed loading. The findings suggest a hypothetical injury mechanism in which primary fracturing is due to concentrated loading and yields a discontinuous decrease in global stiffness, causing successive load concentration on the neighbouring ribs. Consequently, successive fractures occur in the manner of a chain-reaction, or domino effect. The fractures from R4 to 8 could support the hypothesis if the process of the fracturing is considered. However, in comparison with the hotspots in the non-fracture model, it was observed

that the distribution and timing of the fracture in both human models showed a close match. Moreover, a series of fractures occurred almost simultaneously in both human models. This suggests that the change in thoracic stiffness due to the primary fracture did not predominantly contribute to the following fractures, thus the hypothesis was not to be applicable. Taking a look at the kinematics of both human models, it was observed that the fractures were distributed in the region that contacted the left upper arm. This suggests that a vertically distributed load was applied to the side of the thorax. The authors have judged that the results are consistent with the findings from their previous study, which showed that the global stiffness of the rib-cage was higher under vertically distributed loading conditions than in concentrated conditions. Further observation of fractures or hotspots at the time in both human models indicates that the second-phase fractures, i.e. hotspots in R7, 8 and 9 were predicted at t=29-50 ms in the non-fracture model on the side thorax, whereas the fracture model did not simulate them. The authors judged that this was because the load-path was maintained after the occurrence of the first-phase fractures in the non-fracture model, and the regions where the second-phase fractures were predicted were indirectly loaded after the primary fractures.

Next, the authors moved on to the observations of the fractures or hotspots in Case 1. In the fracture model, the first-phase fractures occurred in R8, 9 and 10 on the posterior thorax from t=25 ms, and in R5, 6 and 9 on the side thorax almost at the same time. Moreover, the second-phase fractures occurred in R7, 9 and 10 on the anterior thorax from t=34 ms. In the non-fracture model, hotspots were observed in R4, 5, 6, 8, 9 and 10 on the anterior thorax from t=29-34 ms, but the second-phase fractures were not predicted. Based on an observation from the condition (larger deformation of door inner panel at the seated position), the timing of the fractures and the comparison with the distribution of the hotspots in the non-fracture model, the second-phase fractures are thought to be due to the decrease in thoracic stiffness caused by the first-phase fractures, which could be explained by the hypothesized mechanism described in the discussion of Case 3, i.e. the chain-reaction.

Finally, the authors observed the fractures or hotspots in Case 5. In the fracture model, the first-phase fractures were observed in R4, 5, 6, 7, 8, 9 and 10 on the anterior and the posterior thorax from at t=17-25 ms. Furthermore, second-phase fractures were observed in R2, 3, 4, 5, 6 and 8 on the side thorax at t=42-48 ms. From the comparison with the fracture model, the distribution and the number of fractures in both human models indicated a close match. The authors hypothesize that the first-phase fractures were due to contact with the upper arm and the second-phase fractures were due to contact with the B pillar of the vehicle model, and the timing of the respective applied load is fully isolated (interval of 20 ms). Thus the change of the load-path due to the first-phase fractures did not contribute to the second-phase fractures, in other words, two phases of the fractures were independent phenomena. These observations suggested that the non-fracture model is able to predict the first-phase fractures (a series of fractures that primarily occur after the initiation of the impact) as well as the fracture model. However, in certain specific cases, it might not represent the condition after primary fractures occurred, i.e. the distribution of the second-phase fractures both in a single rib and in the neighbouring ribs. In cases where the causes of the first-phase and the second-phase fractures were independent of each other, such as two isolated loadings, the prediction of the fractures would indicate good correlation in both models.

Previously, the authors conducted simulated side impact experiments and compared the responses of the fracture and non-fracture FE human body models in a specific condition [10]. The results of the study indicated that the number of predicted fractures in both human models indicated a close match, which support the appropriateness of the probability-based method for injury quantification proposed by [11].

In the present study, the predicted first-phase fractures in both human models indicated a good correlation regardless of seated position. The number of fractured ribs in both models indicated a good correlation as well. These results are judged to support the previous study. The results suggest non-fracture FE human body models will be able to predict the Abbreviated Injury Scale (AIS) index with sufficient accuracy, because the AIS currently used classifies the injury severity of the thoracic fracture based on the number of fractured ribs. Previously, [19] predicted the risk of rib-fractures during frontal crashes using measurements from a non-fracture FE human body model and compared the data to real-world data. In their analysis, the prediction based on the measurement of the shear stress and the first principal strain on the FE human body model overestimated the risk of rib fractures under conditions of higher impact velocities. The present study also suggests that the non-fracture model could possibly indicate underestimation of second-phase fractures, due to a decrease in thoracic stiffness caused by the initial-phase fractures, as well as overestimation due to unrealistic

representations of the load-path during the post-fracture period, which the authors observed in their previous study [10], as did [19]. Previously, [20] examined the influence of the arm position on the thoracic response and rib fracture during side impacts using PMHS experiments. They reached the conclusion that the arm position of the impacted side contributed to the distribution of the rib fracture and AIS value. However, the impact conditions they examined were limited in simplified planar loading. During real-world side impacts, the local deflection of the white-body and the interaction with the restraint system may directly affect the loading condition on the thorax, and the arm position which may possibly contribute to the loading condition. These suggest that the loading condition on the thorax during side impacts is more complicated than in frontal impacts because many contributive factors could be combined; the post-fracture response of the rib-cage could vary depending on the case.

Regarding age-related injuries, multiple fractures in a single rib should be considered from the viewpoint of the evaluation of the negative permanent outcome or the Life Years Lost. From that viewpoint, an accurate prediction of age-related injuries with higher bio-fidelity based on both the fracture and non-fracture FE human body models would be worth addressing.

Limitations

The elderly FE human body model used in the present study has not yet been validated against the response from experimental results due to the lack of literature regarding whole body experiments using PMHS of age 75 YO or older. Moreover, due to the lack of available literature, the range (the age-specific or the individual variation) of the material property of the intercostal muscles was not incorporated into the human body models used in the present study. These limitations may possibly reduce the bio-fidelity of the post-fracture kinematics and the distribution of the second-phase simulated fracture in the fracture model; the contribution of the variation of the respective material properties should be evaluated for further analysis.

V. CONCLUSIONS

A series of simulated side impact experiments were performed using fracture and non-fracture elderly FE human body models placed in various seated positions. The predicted fractures from both human body models were compared and analysed. The results indicated that the prediction of the first-phase fractures showed good correlation in both models, whereas the non-fracture model did not represent the distribution of the second-phase fractures observed in the fracture model in the single rib or in the neighbouring ribs. In cases where the causes of the first-phase and the second-phase fractures were independent, the prediction of the fractures indicated good correlation in both models. The results of the study support the appropriateness of the probability-based method for injury quantification.

VI. REFERENCES

[1] Zhou Q, Rouhana S, Melvin J. Age effects on thoracic injury tolerance. *Proceedings of Stapp Car Crash Conference*, 1996, Albuquerque, New Mexico, USA.

[2] Fayon A, Tarriere C et al. Thorax of 3-point belt wearers during a crash (experiments with cadavers), *Society of Automotive Engineers*, 2009, Detroit, Michigan, USA.

[3] Prasad P. Biomechanical basis for injury criteria used in crashworthiness regulations. *Proceedings of IRCOBI Conference*, 1999, Sitges, Spain.

[4] Ito O, Dokko Y, Ohhashi K. Development of adult and elderly FE thorax skeletal models. *Society of Automotive Engineers*, 2009, Detroit, Michigan, USA.

[5] Dokko Y, Ito O, Kanayama Y, Ohhashi K. Development of human lumbar spine FE models for adult and the elderly. *Society of Automotive Engineers*, 2009, Detroit, Michigan, USA.

[6] Dokko Y, Ito O, Ohhashi K. Development of human lower limb and pelvis FE models for adult and the elderly. *Society of Automotive Engineers*, 2009, Detroit, Michigan, USA.

[7] Ito Y, Dokko Y, Mori F, Motozawa Y, Ohhashi K. Kinematics validation of age-specific restrained 50th percentile occupant FE models in frontal impact. *Society of Automotive Engineers*, 2012, Detroit, Michigan, USA.

[8] Dokko Y, Yanaoka T, Ohhashi K. Validation of age-specific human FE models for lateral impact. *Society of Automotive Engineers*, 2013, Detroit, Michigan, USA.

[9] Ito Y, Motozawa Y, Mori F. Response analysis of thoracic cage against blunt loading using human FE Model. *Proceedings of IRCOBI Conference*, 2013, Gothenburg, Sweden.

[10] Motozawa Y, Ito Y, Mori F. Comparison of whole body kinematics between fracture and non-fracture finite element human body models during side impact, *Proceedings of IRCOBI Conference*, 2015, Lyon, France.

[11] Forman J, Kent R, Mroz K, Pipkorn B, Bostrom O, Segui-Gomez M. Predicting rib fracture risk with whole-Body finite element models: development and preliminary evaluation of a probabilistic analytical framework. *Annals of Advances in Automotive Medicine*, 2012, 56:pp.109-24.

[12] Kent R, Lee S et al. Structural and material changes in the aging thorax and their role in reduced thoracic injury tolerance. *Stapp Car Crash Journal*, 2005, 49:pp.231-49.

[13] Gayzik F, Yu M, Danelson K, Slice D, Stitzel J. Quantification of age-related shape change of the human rib cage through geometric morphometrics. *Journal of Biomechanics*, 2008, 41(7):pp.1545-54

[14] ESI Group, H-model™ Version 2007 User's Manual, pp.100-2, *ESI Group*, 100-102 Avenue de Suffren 75015, Paris, France, 2007.

[15] Kroell C, Schneider D, Nahum A. Impact tolerance and response of the human thorax. *Society of Automotive Engineers*, 1971, Detroit, Michigan, USA.

[16] Kroell C, Schneider D, Nahum A. Impact tolerance and response of the human thorax II. *Society of Automotive Engineers*, 1974, Detroit, Michigan, USA.

[17] Lessley D, Salzar R et al. Kinematics of the thorax under dynamic belt loading conditions. *International Journal of Crashworthiness*, 2010, 15(2):pp.175-90.

[18] Rhule H, Maltese M, Donnelly B, Eppinger R, Brunner J, Bolte J IV. Development of a new biofidelity ranking system for anthropomorphic test devices. *Stapp Car Crash Journal*, 2002, 46:pp.477-512.

[19] Mendoza-Vazquez M, Jakobsson L, Davidsson J, Brolin K Östmann M. Evaluation of thoracic injury criteria for THUMS finite element human body model using real-world crash data. *Proceedings of IRCOBI Conference*, 2014, Berlin, Germany.

[20] Kemper A, McNally C, Kennedy E, Manoogian S, Duma S. The influence of arm position on thoracic response in side impacts. *Stapp Car Crash Journal*, 2008, 52:pp.379-420.

VII. APPENDIX

TABLE A I

REPRESENTATIVE MATERIAL PROPERTIES OF FE ELDERLY HUMAN BODY MODEL

Bones		Yield Stress (MPa)	Yield Strain	Ultimate Stress (MPa)	Ultimate Strain
Rib	Cortical	54.0	0.0070	68.3	0.0212
	Trabecular	1.25	0.0061	1.25	1.00
Clavicle	Cortical	80.4	0.0100	97.7	0.0350
	Trabecular	1.25	0.0061	1.25	1.00
Sternum	Cortical	54.0	0.0070	68.3	0.0212
	Trabecular	1.25	0.0766	1.25	0.100
Costal Cartilage		1.27	0.092	1.27	1.00
Intercostal muscle		Bulk Modulus: 2.1 (MPa)			
Internal Organs					
Bulk Modulus (MPa)		Short Time Shear Modulus (MPa)		Long Time Shear Modulus (MPa)	
0.022		2,000		750	

TABLE A II

BIOFIDELITY SCORES OF LATERAL AND VERTICAL DISPLACEMENT FOR BODY REGIONS IN FE ADULT HUMAN BODY MODEL DURING SIDE IMPACTS. (<1: EXCELLENT, <2: GOOD, <3: MARGINAL, >3: POOR)

	Lateral	Vertical
Head	0.40	0.86
T 1	0.37	0.66
T 6	0.23	0.94
T 11	1.00	1.70
L 3	1.18	1.79
Pelvis	0.94	0.71

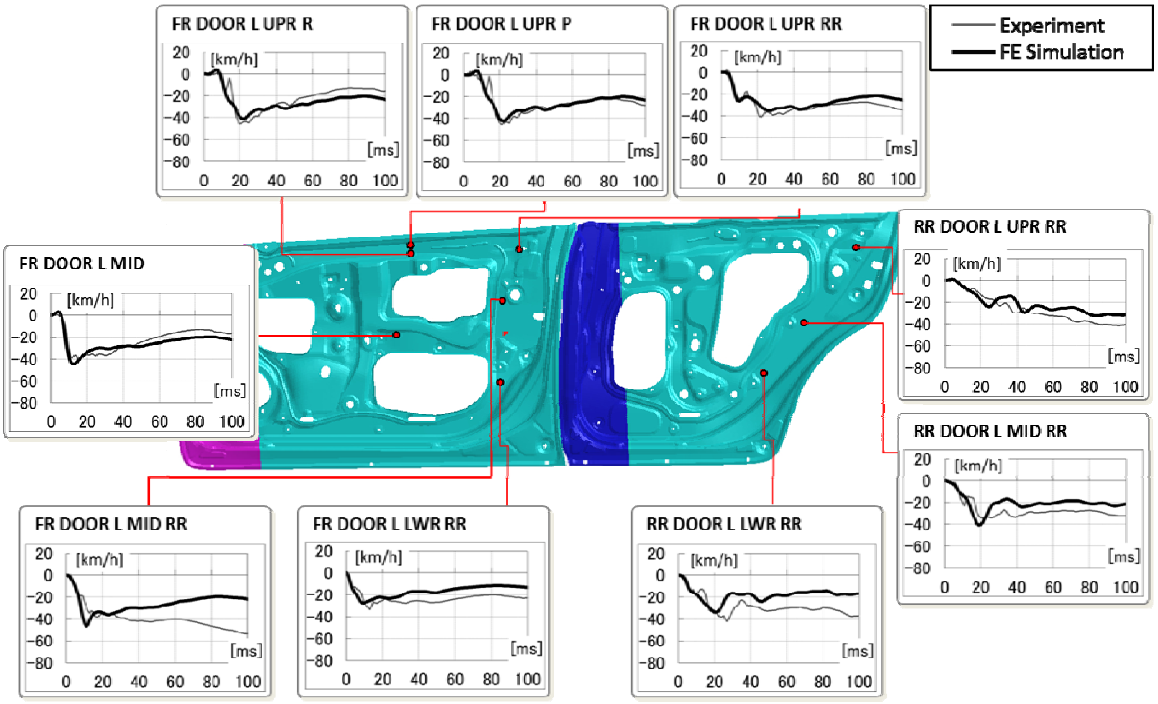

Fig. A1. Comparison of time histories of local velocity measured on doors between experiment and FE simulation.

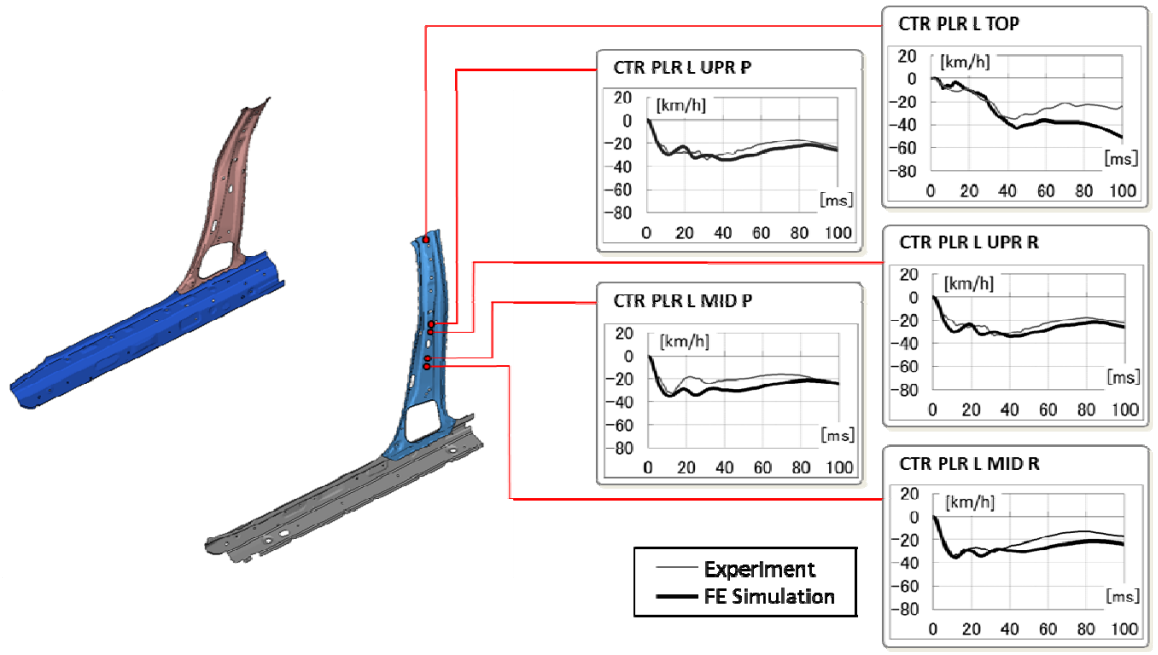

Fig. A2. Comparison of time histories of local velocity measured on B pillar between experiment and FE simulation.